Available online at www.sciencedirect.com
ScienceDirect
Journal of Hazardous Materials 149 (2007) 418–431
Journal of Hazardous Materials
www.elsevier.com/locate/jhazmat

Effect of Pb-rich and Fe-rich entities during alteration of a partially vitrified metallurgical waste

N. Seignez [a,b], A. Gauthier [a,*], D. Bulteel [b], M. Buatier [c], P. Recourt [a], D. Damidot [b], J.L. Potdevin [a]

[a] Université de Lille 1, UMR CNRS 8110, Processus et Bilans des Domaines Sédimentaires, Bâtiment SN5, 59655 Villeneuve d'Ascq Cedex, France
[b] Ecole des Mines de Douai, Département Génie Civil, 941 rue Charles Bourseul, BP 838, 59508 Douai, France
[c] Département de GéoSciences, UFR Sciences et Techniques, 16 route de Gray, 25030 Besançon, France

Received 19 January 2007; received in revised form 26 March 2007; accepted 2 April 2007
Available online 5 April 2007

Abstract

Lead blast furnace (LBF) slags are mainly composed of an iron–silica–lime glass matrix and minor phases such as solid solutions of Mg–Cr-rich and Fe–Zn-rich spinel crystals, crystallized iron oxides such as wüstite and metallic lead droplets. In this study, results from Raman spectroscopy, transmission and scanning electron microscopy allow to argue that widely submicron iron-rich phases are very common in the glass matrix and could have an effect on the general alteration pattern of the glass matrix during leaching experiments. Open flow tests also point out close relationships between glass alteration ability and the presence of large lead droplets. According to numerous papers on nuclear glass leaching, acidic pH encountered in such open flow tests lead to preferential releases of the main alkali-earth metal composing the glass. Altered glass is mainly characterized by relative enrichments in iron. It is induced by high calcium or calcium–silicon depletions. Surprisingly, such type of alteration layer is not uniformly spread on the slag surface. In this work, it is also assumed that previous chemical analyses of the LBF glass matrix having micrometric resolution cannot give a realistic glass composition. A short discussion is also proposed about which characterization techniques can be used to correctly identify submicron iron-rich entities and evaluate their proportions and composition.

Keywords: Slag; Leaching; Glass–ceramics; Altered layer; Nanometric Fe-rich crystals

1. Introduction

Zinc and lead metallurgical plants frequently generate partially vitrified wastes [1–3]. Such wastes often are primary or secondary smelting slags. They are stemming from the barren part of the exploited ores and also contain some additives used in the smelters. The barren liquid is quenched just after the ore treatment. According to their residual heavy metal contents and the environmental hazards they represent, slags can be recycled or just landfilled. In the vicinity of old metallurgical plants, such wastes are generally landfilled on sprawling slag heaps and are exposed to weathering conditions. In this work, only Lead Blast Furnace (LBF) slags are taken into consideration [4–6]. They come from an old metallurgical factory near Noyelles-Godault (Northern France). These slags have already been described in the literature by several authors [7–9].

LBF slags are a granulated waste. They are mostly composed of an iron–silica–lime glass matrix (80 vol.%) which still contains high quantities of lead ($m_{PbO} \approx 3\%$) and zinc ($m_{ZnO} \approx 11\%$). They also contain crystallized phases (19 vol.%) such as plurimicrometric dendritic Zn substituted wüstite ($Fe_{0.85-x}\ Zn_xO$ with $0.085 < x < 0.170$) and varied solid solutions of spinel: from the magnesiochromite ($MgCr_2O_4$) to the franklinite ($ZnFe_2O_4$) and magnetite ($Fe^{2+}Fe_2{}^{3+}O_4$) poles. Plurimicrometric metallic lead droplets only represent 1% of the total slag volume. Nevertheless, LBF slags contain neither melilite and pyroxene nor olivine, while they exist in others lead metallurgical slags [10]. It may be induced by a faster quench [11] which inhibits the pyroxene precipitation normally occurring after spinel formation.

Water-LBF slag alteration processes mainly concern glass matrix and metallic lead [4]. In batch tests, secondary lead carbonates (cerussite: $PbCO_3$), calcium carbonates ($CaCO_3$) and

* Corresponding author. Fax: +33 320 434 910.
E-mail address: arnaud.gauthier@univ-lille1.fr (A. Gauthier).

0304-3894/$ – see front matter © 2007 Elsevier B.V. All rights reserved.
doi:10.1016/j.jhazmat.2007.04.007

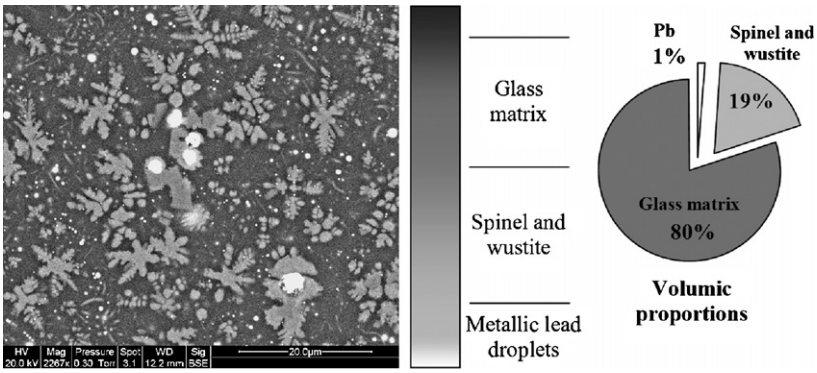

Fig. 1. On the right: SEM backscattered micrograph of LBF slags showing spinel, wüstite and metallic lead embedded into glass matrix. The proportions of each phase are specified on the left.

hydrous ferric oxides (HFO) are usually formed [12,13]. However, crystallized Fe-rich phases appear to be stable in batch tests [4].

A great number of studies have already brought their contributions to glass alteration. They revealed that glass dissolution rate strongly vary depending on factors such as pH [14,15], temperature [16,17], elements in solution (Zn [18]; Pb [19]; Fe [20], Si [15,21], Al [22,23], *S/V* ratio [24,25] flow rate [26–28] and glass composition [29–32].

The last factor strongly influences the glass structure. Indeed, three types of elements are generally taken into consideration: (1) glass formers (e.g. Si, Al, Ge, ...) which participate to the formation of polyhedrons chains together with O_2^-; (2) glass non-bonding elements which are alkali and alkali-earth metal oxides (e.g. Na_2O, CaO, K_2O, Li_2O, MgO, ...). Some elements (e.g. Al, Fe, Pb, ...) are known to play both roles depending on their oxidation states. They are called intermediate elements. Even if the short-range order (0–0.5 nm) is relatively well described with the Continuous Random Network model [33], Modified Random Network model [34] or quite similar models [35,36] are rather used to explain the medium range order (0.5–1.5 nm) in glasses [37,38]. They evoke the micro-segregation of alkalis leading to interwoven sublattices of network regions (composed of network formers) and inter-network regions (composed of network modifiers). These micro-segregations also are described as "cluster pseudophases" spread into a "connective tissue". Then, intermediate element-rich regions play the role of preferential percolation channels [39].

Glass formers usually are localized in sites just a little more distorted than in crystals, e.g. Si or Al bearing tetrahedra [40–42]. Contents of Si and Al occupying other coordinated sites (e.g. five-fold) are generally negligible. According to Ref. [43], glass network is more or less polymerized with various proportions of TO_4 tetrahedra in Q^3 or Q^4 species depending on SiO_2 contents. Q^n is the number of bonding oxygen per TO_4 tetrahedron. Glass modifier such as Na^+ and Ca^{2+} are known to have a depolymerization effect on SiO_2 network [40]. Indeed, Ca^{2+} occupies highly distorted sites [42] and strongly increases the non-bonding oxygen in glass. It leads to a less connected glass network [43]. As for Na [44], Si/Ca ratio has a strong effect on the glass durability in lixiviation tests [30,31].

According to previous studies, iron is usually considered as an intermediate element [43]. Historically, Fe(III) is considered as a network former while Fe(II) is a modifier [11,37]. However, in iron silica glasses containing alkali and alkali-earth metals, ferrous and ferric iron can both occupy four-fold and five-fold coordinated sites generally in association with tetrahedral and trigonal bipyramids [45–47]. Moreover, ferric iron is a little more rigidly bound than ferrous iron [45].

According to Ref. [13], lead droplets lower than 1 μm are present in old lead metallurgical slags. Pb might be entirely contained in micrometric and nanometric lead entities due to liquid–liquid separation phenomena during the melt [4]. Nevertheless, at present, Pb is considered as an element contained in the LBF glass. In glass, lead and zinc are respectively considered as intermediate and glass former [43,48]. Depending on their concentrations, Pb and Si compete to form randomly packed TO_4 pyramid polymeric chains [48,49], while ZnO_4 tetrahedra often are apex connected with SiO_4 tetrahedra [37]. Increasing ZnO contents generally improves glass durability [50]. However, Ref. [30] demonstrates that very low Pb and Zn contents play a negligible role on glass durability.

Phenomena controlling glass dissolution behaviour are pH-specific [14,15,51]. In acid media, selective glass dissolution occurs. Such preferential cations exchanges, mainly concern alkali and alkali-earth metals. In basic pH, glass dissolution is congruent. In batch experiments, cations exchanges rapidly contribute to a pH increase which leads to the succession of the both mechanisms. It can lead to the formation of a dense gel with protective properties [52–56]. Nevertheless, stability of such a gel is usually strongly affected by the native presence or the secondary formation of clay minerals. Indeed, these phases contribute to a continuous transfer of glass constituents from the gel to the leachate [53,54].

The aim of this work is: (1) to study the general alteration pattern of the LBF glass during an open flow experiment and (2) to discuss about the presence of Fe-rich and Pb-rich entities and their influences onto glass alteration. Results are compared to previous works dealing with Fe-rich phase in annealed vitreous

Table 1
Slag composition has been estimated by ICP-AES and ICP-MS after meltings and acid attack

	LBF1	LBF2	LBF3	LBF4	Mean
Mass%					
SiO_2	23.61	23.64	23.17	26.51	24.33
Al_2O_3	2.44	2.46	2.48	2.47	2.46
Fe_2O_3	10.73	10.34	10.75	9.69	10.38
FeO	23.01	23.47	23.26	23.52	23.32
MnO	0.81	0.81	0.80	0.80	0.81
MgO	2.74	2.80	2.70	2.61	2.71
CaO	22.29	22.47	21.8	21.83	22.10
Na_2O	0.63	0.64	0.62	0.58	0.62
K_2O	0.37	0.38	0.34	0.27	0.34
TiO_2	0.20	0.19	0.20	0.19	0.20
P_2O_5	0.25	0.29	0.26	0.22	0.26
ZnO	11.46	11.48	11.46	10.04	11.11
PbO	3.67	3.76	3.82	3.27	3.63
S_{tot}	0.38	0.39	0.39	0.38	0.39
LOI	0.46	0.87	0.54	0.43	0.58
Total	102.13	102.25	101.51	101.95	101.98
In mg/kg					
Ag	12	12	13	7.5	11.1
As	780	750	780	717	756.8
Ba	6500	6330	6330	5919	6269.8
Cr	965	965	945	908	945.8
Sn	1425	1410	1430	1275	1385
Ni	72	71	71	83	74.3
Cl	110	106	105	104	106.3
Mo	280	266	274	276	274
Cd	3.5	4	3.2	4.3	3.8
Sr	1680	1680	1600	1572	1633
Hg	<20	<20	<20	<20	–
Se	2.1	2	1.9	2	2
Sb	–	–	–	1389	1389
CO_{2tot}				0.16	

Fe(III) and Fe(II) concentrations are evaluated by titration and S_{tot} and CO_{2tot} by using infrared absorptiometry (Ref. [4]). LOI: Lost on ignition.

wastes and studies concerning metallurgical slag weathering and glass leaching.

2. Materials and methods

2.1. LBF slag

Slag grains generally are black with a vitreous lustre. They do not exceed several millimetre in diameter. Their size is lognormal with a 500 μm dominant class [8]. As previously evoked, LBF slags are mainly composed of a glass matrix. They also contain crystallized phases such as wüstite and solid solutions of spinels and metallic lead droplets (Fig. 1). Minor phases usually are plurimicrometric grains while lead droplets often range between 1 and 100 μm. This waste is mainly composed of three major oxides (SiO_2, CaO and FeO) whose proportions are superior to 20% (in mass) for each one [4]. Contents of Fe_2O_3 and ZnO, respectively, range between 9.69 and 10.73% and between 10.04 and 11.48% (in mass). PbO contents are relatively lower, i.e. 3%, while other oxides like Al_2O_3, MnO, MgO, Na_2O, K_2O are present in contents lower than 3% (Table 1). Analyses shown in Tables 1–3 indicate that many elements composing LBF slag are both contained in glass matrix and minor phases. Indeed, glass is mainly composed of Si, Ca and Fe. It also contains significant amounts of Zn, Pb and Al (see Table 2). The others oxides (MgO, MnO, Na_2O, K_2O, P_2O_5, TiO_2) often represent less than 2% (in mass). Depending on the spinel type, spinel solid solutions can contain relatively high amounts of Al, Cr, Fe, Mg and Zn (Table 3). Lead entities contain some elements such as Fe, Ag, As, Cu, Sn and Sb in various amounts (from 0.5 to 5% depending on the element in consideration). This is in agreement with Ref. [6] which indicates that for low S contents (≈0.4% in this study) Cu is incorporated into metallic lead. According to these previous measurements, glass composition is quite similar to the global composition of the LBF slags (Table 1).

2.2. Leaching method

Polished sections (60 mm × 20 mm) are placed in a leaching container supplied in pure water (pH 5.6) by a peristaltic pump. It provides a constant flow of 60 ml h^{-1} (Figs. 2 and 3). Slags are only situated on the upper face of the sections and occupy 40% (≈500 mm^2) of it, while the volume of water in the container is approximately 4 cm^3 ($S/V \approx 1.2\ cm^{-1}$). Some containers used in this study allow to alter three sections. In such case, S/V ratio does not notably change. Darcy velocity in the container is about 1 m h^{-1}. The sections have been observed after 15 and 26 days of alteration. The chemical analyses (SEM-EDS and Raman) have been obtained at initial step and after 26 days of alteration. Sampling schedule at the outlet of the container (e.g. 1 sample h^{-1}) and emission spectrometry analyses are quite similar than for the column test developed in Ref. [57]. ICP measurements take into account for the following elements: Si, Al, Fe, Pb, Zn, Mg, Na, Mn, Ca, K, Cr, As, Cu, Ti, Ni, Ba, Cd. The detection level is about 20 μg l^{-1} for all of them except for Cu (50 μg l^{-1}).

2.3. Sample preparation and analytical methods

2.3.1. Polished sections

To avoid any quality depletion during microscope observations (generally cause by roughness at the slag surface), slag grains (size ≥ 1.6 mm) have been embedded in an epoxy resin and polished to plates. During the sample preparation, contact between water and polished sections has been strongly reduced to avoid any early alteration of the most reactive phases such as the lead metallic entities. Thus, waterless abrasive diamond pastes, alcohol lubricants and alcohol rinsing liquids have been preferentially used. To observe lixiviation effects with depth, perpendicular cuttings have been done into altered polished sections. Samples have been embedded in epoxy resin to preserve altered glass layers before perpendicular cuttings.

2.3.2. Electron microscopy

An Environmental Scanning Electron Microscope (FEI Quanta 200, University of Lille) is used to compare glass initial composition together with the altered layer and to observe the general morphology of the slag surface. Its tungsten electron source is used at 20 keV. Elementary analyses are supplied

Table 2
LBF glass composition measured with an electron microprobe (in Ref. [4])

	Mass%									
	D_1	D_2	D_3	D_4	D_5	D_6	D_7	Mean	Min	Max
SiO_2	26.57	26.06	26.03	26.06	27.3	26.57	26.06	26.38	26.03	27.3
TiO_2	0.20	0.24	0.23	0.23	0.19	0.20	0.24	0.22	0.19	0.24
Al_2O_3	2.72	2.34	2.45	2.47	2.72	2.72	2.34	2.54	2.34	2.72
Cr_2O_3	0.02	0.04	0.10	0.01	0.04	0.02	0.04	0.04	0.01	0.10
FeO	27.08	28.1	25.92	25.72	23.51	27.08	28.1	26.5	23.51	28.1
CaO	21.90	22.09	24.82	24.59	23.08	21.9	22.09	22.92	21.90	24.82
MgO	1.70	2.07	2.10	2.12	1.61	1.70	2.07	1.91	1.61	2.12
MnO	0.98	0.92	0.60	0.64	0.86	0.98	0.92	0.84	0.60	0.98
ZnO	11.09	10.11	12.27	12.25	11.2	11.09	10.11	11.16	10.11	12.27
PbO	4.29	4.08	3.76	3.46	6.14	4.29	4.08	4.30	3.46	6.14
Na_2O	0.70	0.88	1.32	1.22	0.63	0.70	0.88	0.90	0.63	1.32
K_2O	0.40	0.37	0.47	0.42	0.38	0.40	0.37	0.40	0.37	0.47
CuO	0.11	0.13	0.05	0.11	0.28	0.11	0.13	0.13	0.05	0.28
SO_3	1.05	0.60	1.10	0.99	1.22	1.05	0.60	0.94	0.60	1.22
P_2O_5	0.18	0.06	0.24	0.22	0.19	0.18	0.06	0.16	0.06	0.24
BaO	0.75	0.91	0.74	0.88	1.00	0.75	0.91	0.85	0.74	1.00
As_2O_3	0.18	0.06	0.07	0.10	0.14	0.07	0.09	0.10	0.06	0.18
Total	99.92	99.06	102.27	101.49	100.49	99.81	99.09			

Table 3
Minimum and maximum contents of several oxides in spinel solid solutions (from Ref. [4])

	Mass%					
	Al_2O_3	Cr_2O_3	Fe_2O_3	FeO	MgO	ZnO
Minimum	0.58	1.55	8.08	4.86	1.92	9.87
Maximum	16.16	44.64	68.02	17.65	12.77	15.91

by an X-ray Energy Dispersive System (EDS) with a Rontec Single Drift Detector (SDD). Its accuracy (in elemental composition) reaches 0.5% in high vacuum mode. However, to keep slag surface free from hard disturbances, polished sections are not carbon coated and observed in low vacuum mode. The pressure in the chamber is relatively low (≤0.45 Torr). It reduces slightly the probe accuracy and as a consequence only global trends of the glass chemistry will be discussed here.

A Transmission Electron Microscope (JEOL1260, University of Franche Comté) is used to observe slag thin sections. They have been prepared by selecting areas on fresh slag thin sections (30 μm). These areas have been disposed on a 2 mm copper grid, ion milled, and carbon coated for TEM investigations. TEM electron source is used at 120 kV.

A Raman spectrometer (Labram-Jobin-Yvon, Horiba Group, University of Lille) has been used to identify Fe-rich and Pb-rich phases in different areas of slag sections at initial step and after the leaching tests. This apparatus is equipped with a 5 mW LASER (λ = 632.8 nm). Spectra acquisition time ranges between 20 and 60 s and the number of iteration ranges between 1 and 3 for each analysis.

3. Results

3.1. Fresh glass

3.1.1. SEM observations

On SEM micrographs in backscattered electron mode (BSE), glass matrix, lead metallic droplets, Fe-rich entities and non-ferrous spinels appear in different light grey levels mainly depending on the atomic weight of the elements which compose them (Fig. 4). Fe-rich entities, e.g. wüstite crystals, mostly are small dendrites. However, other shapes are observed. Different populations of grains are distinguished according to their size. The easiest to observe are the ones whose sizes are superior to 1 μm. However, some grains have a micrometric size or a little smaller size. Each population of Fe-rich entities is homogeneously spread into a given area of glass matrix. Spatial segregations are commonly observed according to the

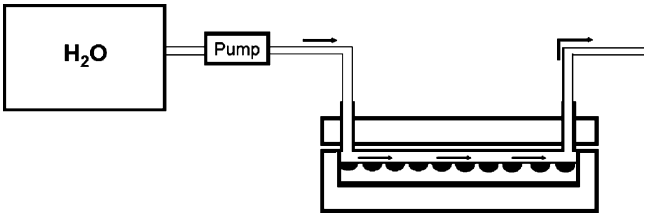

Fig. 2. Scheme of the experimental device.

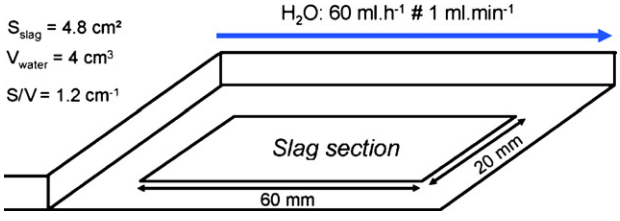

Fig. 3. Detailed scheme of the lixiviation container (inside).

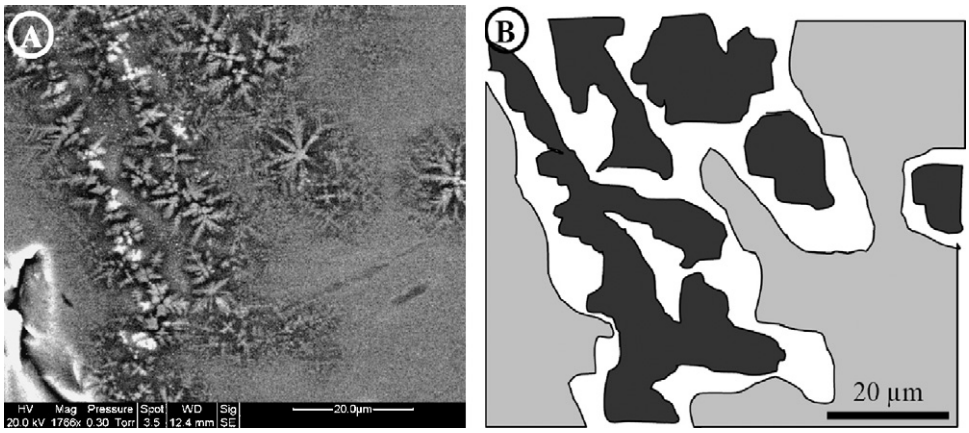

Fig. 4. SEM-BSE micrograph of the glass matrix showing plurimicrometric dendritical iron oxides (A). Spreading of iron-rich entities in the glass (B). Grey: Glass matrix supposed to contain submicron iron-rich entities. Black: Plurimicrometric crystallized iron oxides. White: Glass matrix supposed to be free from iron-rich entities.

population sizes. On SEM-BSE micrographs, due to lower contents in Fe, glass matrix appears always darker than the iron oxides.

However, in some cases glass matrix can have two relatively different grey levels especially in the direct neighbourhood of some plurimicrometric crystallized iron oxides (Fig. 4). This could be due to higher iron contents either incorporated in some zones of the glass matrix or caused by the presence of Fe-rich entities with sizes widely lower than 1 μm.

3.1.2. Glass composition

Fresh glass composition has been analysed on 42 polished grains thanks to SEM-EDS investigations. A total of 168 analyses have been performed with either a spot shape (spatial resolution: 1 μm^3) or several elliptical shapes (>1 μm^3). All the analysed zones have been randomly chosen either in dark glass regions or in lighter glass regions (supposed to contain more iron). Each analysis has been carried on zones characterized by homogeneous contrast in BSE mode. Results concerning SiO_2, CaO and FeO contents are plotted in a ternary diagram (Fig. 5). Iron contents are given in FeO mass percents though Fe(III) may exist in the glass matrix. All these analyses are grouped around the centre of the diagram suggesting that these results are relatively comparable to the microprobe analyses (Table 2). Nevertheless, iron contents strongly vary from a zone to another and as a consequence the analyses can be split into two parts. The first group ranges between 35 and 48% FeO. The second group only ranges between 26 and 35% FeO. In BSE mode, grey levels and iron contents are clearly correlated. Indeed, lighter grey levels are observed with greater amounts of heavy elements. This confirms that iron highly contributes to grey level variations in glass.

In glass areas with grey levels suggesting higher iron contents, Raman analyses often show a peak at 671 cm^{-1} (Fig. 6). Peaks near 671 cm^{-1} strongly suggests the presence of wüstite and/or magnetite [58]. The fluctuations reported in the litera-

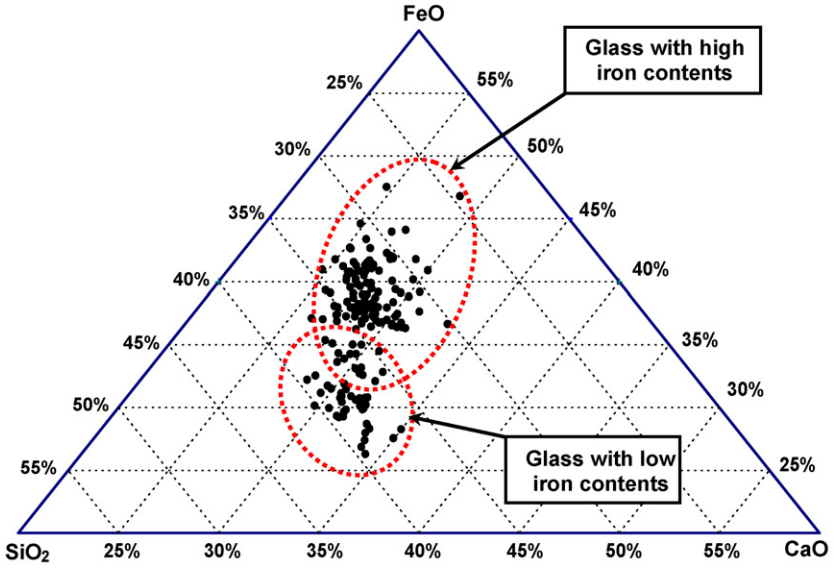

Fig. 5. Ternary diagram showing SEM-EDS analyses of the fresh glass (in mass%).

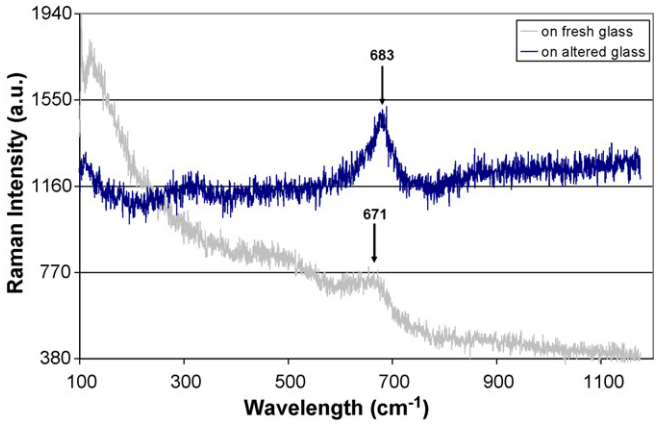

Fig. 6. Raman spectra of a fresh and an altered glass. They suggest submicron iron-rich entities in the glass bulk. Altered glass spectra have been acquired in a similar zone than the one located around the analysis point P4 (see Fig. 9A).

ture could be temperature dependant or could be specific to the laser power [58]. Several altered glass areas give similar results (Fig. 6) than in the fresh glass. These observations tend to validate our second hypothesis, i.e. the presence of widely submicron Fe-rich grains in the glass matrix in zones which appears in lighter grey levels.

3.1.3. TEM observations

Some TEM micrographs show entities at the nanometre scale (Fig. 7). They are dendritically shaped approximately such as micrometric wüstite observed in SEM-EDS (Fig. 4). Their size does not exceed 60 nm. According to the results obtained in SEM-EDS and Raman spectroscopy, it can be supposed that they are Fe-rich entities. On the observed areas (several square micrometres), repartition of these Fe-rich entities look like homogeneous. These micrographs indicate that chemical analyses by EDS with a SEM have to be interpreted with care. Indeed, such phases are taken into account in the analysed volume in SEM-EDS or microprobe analyses (resolution near 1 μm^3).

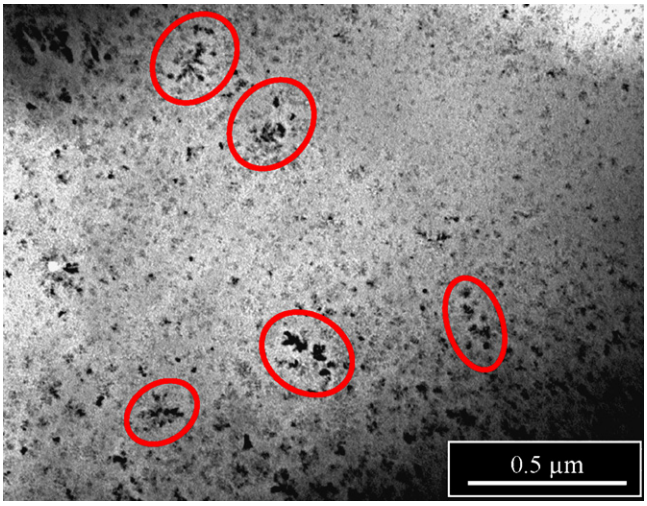

Fig. 7. Transmission electron micrograph of a glass area containing nanometric iron-rich entities. Circled zones indicate the more individualized of such entities (dark dendrites).

3.2. Lixiviation experiments

3.2.1. Leachate chemistry

Emission spectrometry analyses reveal that leachate chemistry at the outlet of the container is quite similar to pure water. Element concentrations often are under the detection level and/or rarely reach concentrations encountered in the blanks. Despite pure water does not buffer the experiment and that pH can evolve during leaching [25,31], some pH analyses indicate a pH near pure water which is relevant with emission spectroscopy measurements. Considering flow rate and water volume in the container, it can be assumed that residence time is very low in the container (i.e. 5 min). Moreover, *S/V* ratio is relatively low compared to *S/V* (=21 cm^{-1}) in some others column tests [57]. Indeed, it has been demonstrated that using 150 g of slags (grains sizes: 2–2.5 mm) and for a residence time of 1 h in the column test (flow rate: 60 ml h^{-1}) only Ca, Si, Pb and Zn are released but in relatively low concentrations (less than 500 ppb for Ca and Si, less than 200 ppb for Pb and Zn) when an apparent steady state is reached [57]. Concerning pH values, the same trend is observed in the evoked column experiment and the polished section tests. Indeed, in the column test, pH rapidly reaches a value near pure water pH. In spite of this indication, it could be assumed that laminar flux in such polished section tests could generate disturbances (fluctuations) of the pH value near slag surface. Indeed, "water layers" could be partially motionless in this area. However, it can be kept in mind that alteration occurs in an acidic near neutral system.

In the column test [57], alteration figures in the glass matrix are encountered just at the column inlet, where water is more corrosive. This concerns a very low amount of grains. Upper grains are less altered in the column. It can be assumed that such polished sections reproduce conditions encountered at the column inlet.

3.2.2. Precipitations of secondary phases

Only two types of lead carbonates precipitate during alteration (Fig. 8A and B). Hydrocerussite ($Pb_3(CO_3)_2(OH)_2$) and cerussite ($PbCO_3$) have been identified on Raman spectra (Fig. 8C) by comparison with data given in another study [59]. Very low quantities of lead carbonates are formed: regions with a lot of lead carbonate crystals (like the one shown in Fig. 8A) have been observed only twice during the polished section experiments. Crystals are generally disposed around the large metallic lead droplets (>150 µm) which are organized in groups of two or three droplets. These carbonate crystals range between 20 and 50 µm. Their sizes can occasionally reach a length of 100 µm. Raman spectra combined with SEM micrographs show that small crystals of cerussite and hydrocerussite have grown at the surface of big metallic lead droplets. Experimental conditions encountered in the polished section tests (including pH) allow the formation of lead carbonates [60,61]. However, this phenomenon is not marked. When the conditions are favourable and when lead carbonates are formed, glass is generally kept from alteration at the surrounding of metallic lead (see Figs. 8A and 9D for comparison). This suggests relationships between the precipitation of lead carbonates and the glass matrix preservation.

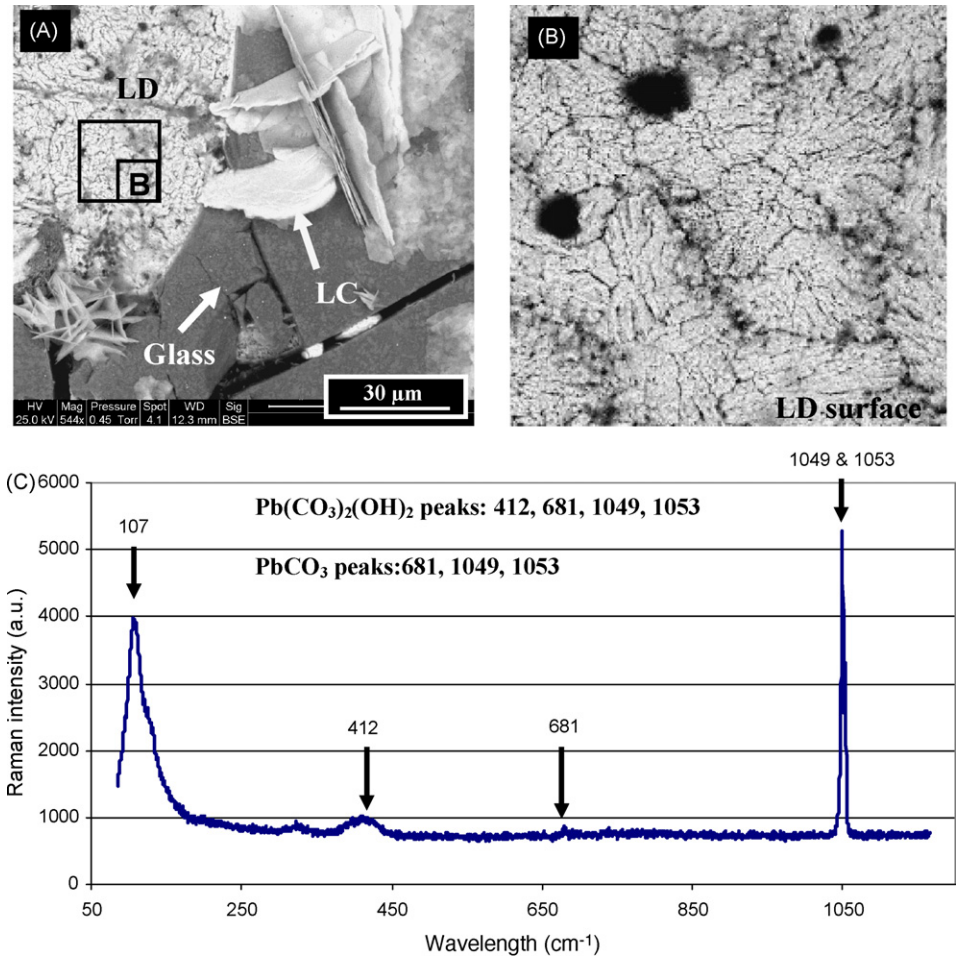

Fig. 8. SEM-BSE micrograph showing lead carbonates around a group of metallic lead droplets after 15 day alteration (A). SEM-BSE micrograph showing the surface of an altered droplet covered with lead carbonates (B). LC: Lead carbonates; LD: lead droplets. Typical Raman spectrum of such secondary phases (C).

Sources of CO_3^{2-} can be both slag alteration ($CO_{2tot} = 0.16\%$ in slags [4]) or caused by dissolution of CO_2 into pure water when in contact with air in the pure water tank. It is possible that the small lead carbonates growing on the droplets progressively cover them and protect the lead droplets from further dissolution.

3.2.3. Surface morphology

After 15 and 26 days of leaching, alteration does not homogeneously affect glass matrix on the polished sections. On the glass surface, three types of areas are distinguishable (see Fig. 9): (1) areas with important alteration marks (i.e. abundant cracks), lighter grey levels on SEM-BSE micrographs and formation of micro-canyons (Fig. 9A and B); (2) regions with less glass alteration evidences. These regions are only affected by cracks appearing next to the plurimicrometric dendritically shaped oxides (see Fig. 9C); (3) in a lot of other cases, SEM-BSE micrographs do not reveal any obvious trace of glass alteration. SEM micrographs show that glass matrix is totally free from any crack before leaching. Then, cracks are not induced by polishing or sawing methods during sample preparation. It seems to be related to the dessication of a hydrated altered layer in the SEM chamber during the investigations. This altered layer obviously is the alteration product of the fresh glass matrix.

The proportion of each type of areas described above cannot be correctly estimated. The different types of areas have generally small dimensions and are randomly distributed. These three types of zones have no identification criteria which could allow quantification by means of image analysis. However, SEM micrographs have shown that the unaltered zones and the poorly altered ones dominate the grain surfaces, compared to the altered and highly altered zones.

The highly altered zones can be located near or far from the metallic lead droplets which are often partially or totally altered. The alteration characteristics can be different according to the proximity of the droplets.

Micro-canyons are often visible at the glass surface in the highly altered zones far from the droplets (Fig. 9A and B). The glass deep in the micro-canyons can be darker than the surrounding glass which composes the edge of the canyon. Glass at the bottom of the canyons is also generally highly fractured. The micro-canyons are probably created both by physical effects (water flow erosion) and by the chemical evolution of the glass surface. Other zones (e.g. Fig. 9A, analysis point P2) are located in the micro-canyon but with an “altitude” near the surface of the micro-canyon edges. These zones appear in very light grey levels. Are they less altered than glass deep in

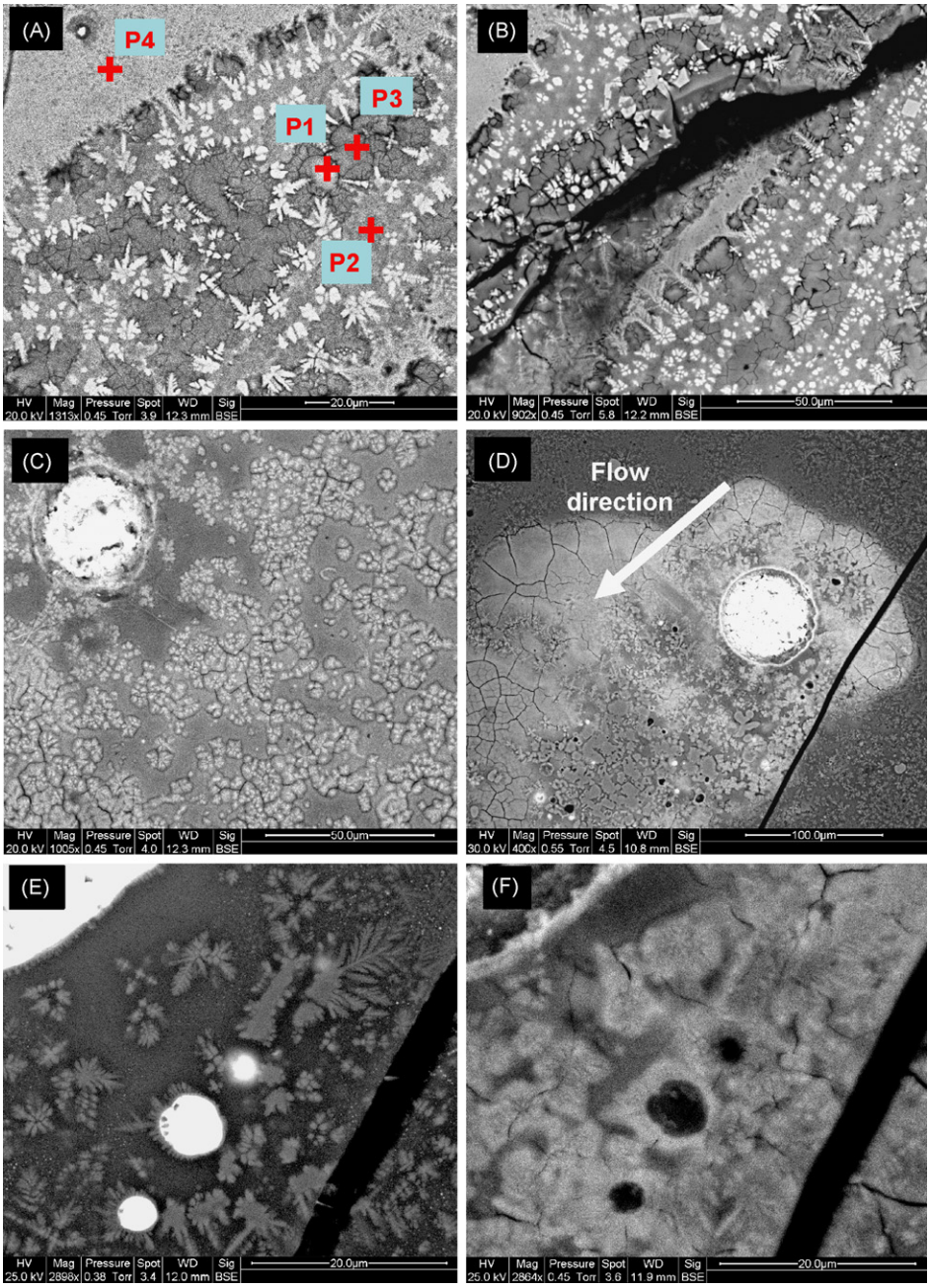

Fig. 9. (A and B) Glass alteration zones which are not under the influence of lead droplets. On micrograph (A), four EDS analyses are localized (corresponding analyses, see Fig. 9). On micrograph (C), there are less glass alteration evidences: only some cracks appear next to the plurimicrometric crystallized oxides. Micrographs (D–F) show glass alteration next to lead droplets. In particular, (E and F) show the evolution of glass matrix and crystallized iron oxides between the initial step (E) and after 26 days of alteration (F).

the micro-canyons? Their chemical compositions are discussed below.

Sometimes, the edges of the micro-canyons appear in very light grey levels. They show a very dense network of crystallized iron oxides which are often freed from the glass by corrosion during leaching tests. Raman analyses of these zones are very similar to the Raman spectra of fresh glass matrix (Fig. 6). These associations of glass and Fe-rich entities (at micrometric scale or lower dimensions) are not always visible before alteration owing to the limit of the SEM resolution and quite similar grey levels between iron oxides and glass supposed to contain submicron Fe-rich entities.

3.2.4. Glass chemical evolution

SEM-EDS analyses of fresh, altered and apparently unaltered glass matrix are plotted in a ternary diagram (Fig. 10). This graph shows that in general morphologically affected regions are also chemically affected (determined by comparison with fresh glass). In such altered glasses, Ca and Si contents strongly decrease. In certain cases, calcium loss is predominant compared to Si loss. However, the decrease of Ca and Si may be simul-

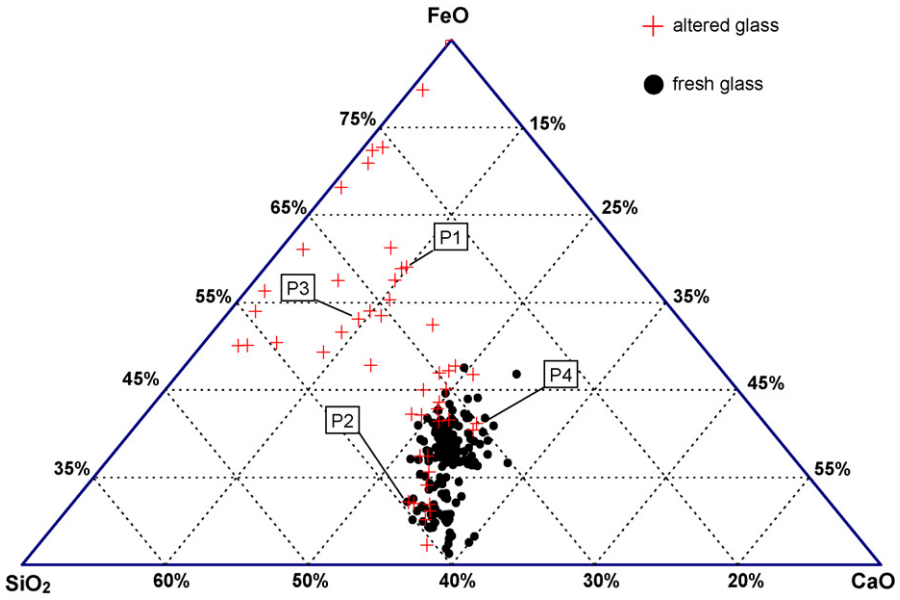

Fig. 10. Ternary diagram showing analyses of the fresh and altered glass (in mass%). Analyses named P1, P2, P3 and P4 are localized in Fig. 9A.

taneous. At maximum, Ca contents can be affected by a fall of 85% compared to the initial contents. Nevertheless, when Ca contents reaches 7% (in mass), the loss of Ca apparently stops. Only the loss of Si continues. The loss of Si can reach 75% compared to the initial contents. This leads to a relative enrichment in iron contents in the glass altered layer. Iron content can reach 80%. According to the lower iron content measured in a fresh glass, iron content in the altered layer can be multiplied by 2.2 at maximum.

In some zones of the altered polished sections, chemical composition of the glass does not evolve. It is often the case for glass areas without morphological evolution or which show only some rare cracks at the proximity of iron-rich entities. Glasses whose chemistry strongly evolves generally present the most intense morphological evolution. For example, several observations indicate that the most intense Ca and Si losses are situated in the micro-canyons (e.g. Figs. 9A and 10, analysis points P1 and P3), in particular, where the glass is the most fractured. In spite of high Ca and Si losses in the micro-canyons, they are darker than they should be on SEM-BSE micrographs. Indeed, considering the relative increase of the iron contents, glass should tender the glass matrix lighter on micrographs. This could be due to shadow effects provoked by surface relief or the decrease of the glass density during the alteration.

Regions of the micro-canyons (higher and very light) have been analysed (e.g. Fig. 9A, analysis point P2). These analyses are located in the lower parts of ternary diagram (Fig. 10). It corresponds to the composition of a fresh glass supposed to be free from or less affected by unobservable Fe-rich entities. This type of glass has no significant Ca and Si loss and then, no iron enrichment. Its alteration is less advanced compared to the glass deep in the micro-canyons. Yet, its properties suggest that this type of glass can identically be altered.

Zones which constitute the borders of the micro-canyons often are glass matrix areas with a very high content of plurimicrometric Fe-rich entities (Fig. 9A, analysis point P4). Sometimes, they show small holes induced by the dissolution of rare glass areas. The chemical compositions of such zones are similar to these of the second group of fresh glass characterized by higher iron contents (see Fig. 5).

3.2.5. SEM-EDS cartographies

SEM-EDS cartographies confirm the tendencies observed in Fig. 10. Fig. 11A shows strongly altered glass just around a small lead droplet (10 μm). In addition to Si and Ca depletions (Fig. 11B and C), and Fe enrichment (Fig. 11D), it also shows that Pb contents are higher in the altered glass than in the apparently unaltered regions (Fig. 11E). It is in accordance with lighter grey levels in the altered zone. However, these lighter grey levels can be also induced by Fe enrichments. Pb enrichments could be only due to Pb stability in such experimental conditions. Nevertheless, Pb enrichment in the altered zones is not observed on every highly altered glass. Thus, even if Pb was stable in glass, lighter grey levels would not be induced by a supposed native lead enrichment in the altered glass.

No lead carbonates have been observed on the altered glass. It could be assumed that lead adsorption occurs at the slag surface. Indeed, such relative increase of lead content can be in accordance with the vitreous network discharge of the Ca cations [60,62]. These authors indicated that in these conditions (relatively acidic pH), sorption phenomena and lead carbonate formation can exist at the same time. In the case presented here, the reaction kinetics promotes the adsorption reactions [61].

3.2.6. Influence of Pb-rich entities

Altered glass also can be highly altered without creation of distinguishable micro-canyons. Such altered zones are generally observed near isolated droplets of medium or large size (e.g. >150 μm). Glass evolution is a bit different compared to glass deep in micro-canyons (Fig. 9D). Glass matrix and Fe-rich enti-

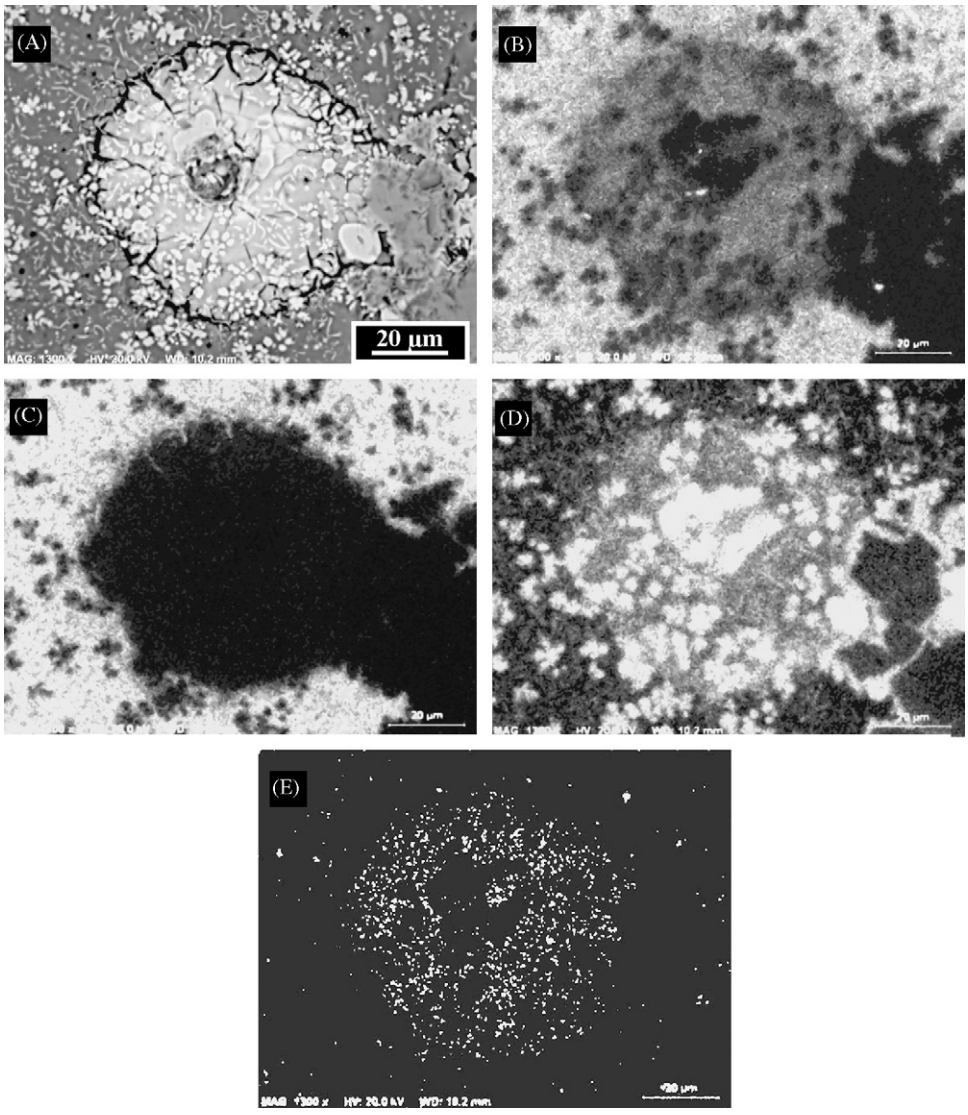

Fig. 11. SEM-BSE micrograph of an altered glass at the surrounding of a lead droplet (A) and the corresponding EDS cartographies of iron (B), silicon (C), calcium (D) and lead (E).

ties around the droplets are lighter on SEM-BSE micrographs. Cracks are abundant in the glass near plurimicrometric Fe-rich dendrites. This lighter area near the droplet has often a plume shape. The orientation of the plume and the fluid flow direction are similar. This suggests a relationship between the fluid flow direction in the reactor and the localization of the glass alteration. Metallic lead dissolution generally tends to increase the pH of the aqueous phase; thanks to the following reaction (see MINTEQ database):

$$Pb_{(metal)} + 2H^{+} + \tfrac{1}{2}O_{2(aq)} \rightarrow Pb^{2+} + H_2O$$

The local influence of lead droplets is clearly proven here. The lighter grey levels of the glass can suggest a relative increase of Fe and/or Pb content. The relative content of iron could be explained by the loss of Ca and Si in the glass matrix. Unfortunately, glass composition in such zones often is difficult to measure by SEM-EDS. Indeed, glass areas containing Fe-rich entities often are predominant.

Around such alteration plumes, glass matrix strongly evolves at the proximity of plurimicrometric iron oxides (Fig. 9E and F). The glass/iron oxide limits become very hard to distinguish. Such an evolution is only observed near medium isolated lead droplets and could also suggests sorption effects concerning Pb or other elements (e.g. Zn) at the surface of the iron oxides and others crystallized phases [63–65].

3.2.7. Alteration profile

In order to study the alteration effects in depth into the glass, vertical cuttings have been prepared on polished sections (Fig. 12). The polished sections used here are smaller and have been altered in smaller containers than presented in Figs. 2 and 3. However, conditions of alteration were similar.

In the regions without plurimicrometric dendritical iron oxides, the glass alteration layer has got a relatively constant thickness. The layer often reaches several micrometres (e.g. 10 μm at maximum). However, in some regions where plurimicrometric dendritic iron oxides are spread into the glass,

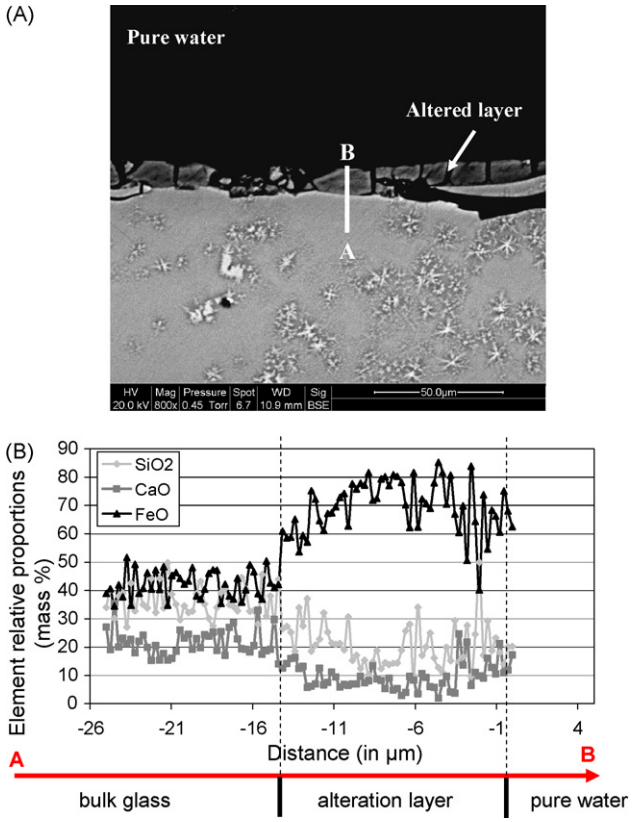

Fig. 12. (A) Vertical cutting in an altered slag. The altered layer appears in darker grey levels. Its thickness approximates 10 μm. (B) SEM-EDS analyses corresponding to the straight line profile [AB] localized in Fig. 11A.

observations have shown that thickness of the altered layer is not constant because of their presence.

SEM-EDS analyses are plotted in Fig. 12B. They are organized as a linescan profile (straight line) vertically drawn on 25 μm from the glass/water interface towards (see AB segment, Fig. 12A). This profile is composed of 100 punctual analyses. The chemical evolution of the glass in depth reveals a preferential depletion in Ca and Si. This leads to the creation of an altered layer enriched in iron (from ca. 40% in the fresh glass to *ca.* 80% in the altered layer). Within the bulk to the interface glass (i.e. from 10 to 0 μm), Fe, Si and Ca contents remain constant.

On SEM-BSE micrograph, the limit between the altered layer and the fresh glass is clear. The Si, Ca and Fe proportions are highly comparable to the previous chemical analyses measured deep in the micro-canyons. As for them, the altered layer is darker than the fresh glass. This strengthens the idea that glass is dark because of the loss of matter and thus of density in the altered zones. It dismisses the idea of shadow effects due to surface roughness in the micro-canyons.

4. Discussion

4.1. Fe(III)/Fe(II) ratio

Previous studies already evoke the role of Fe(III)/Fe(II) ratio in vitrified industrial wastes and in several Fe-rich glasses [11,66]. Notably, formation of magnetite or franklinite crystals can occur by annealing iron reach alkali and alkali-earth silica glass. In the silica melts, the formation of such crystals is particularly abundant when Fe(III)/Fe(II) ratio is kept closed to magnetite stoechiometric values. When six-fold Fe(III) contents are quite high, magnetite formation is doped too [67]. This generally leads to a vitrified waste which contains high amount of Fe-rich entities as for LBF slags.

Fe(III)/Fe(II) ratio strongly depends on parameters like the melt temperature, the melting time, the atmosphere composition and the melt composition [11]. Some elements can also play the role of reducing or oxidizing agents [68]. No evaluation of this ratio has been done on LBF slags. Nevertheless, slag grains are black. This could indicate that glass contains relatively high amounts of ferrous iron. High Fe(III)/Fe(II) ratio would lead to form yellow glasses. Moreover, such type of Zn-rich slags can contain relatively high contents of Fe(II) [6]. These indications point to significant amounts of Fe(II) in the LBF glass matrix. Such conditions could be relevant with the formation of high amounts of very small crystallized iron oxides in the silica melt just before or during the quench.

4.2. Fe-rich entities versus glass composition

Raman spectra and TEM observations show that a significant part of widely submicron Fe-rich entities are included in the glass matrix. Some studies indicate that such phases are commonly encountered in different types of vitrified or annealed iron–silica–lime glasses and ceramics. These Fe-rich crystals are often widely submicronic grains (50–200 nm) of magnetite and franklinite [11,66]. In LBF slags, these entities had not been detected before by SEM micrographs. Glass matrix was interpreted as homogeneous at micrometric scale. Taking into consideration that these entities are widely spread in the glass matrix, both glass composition and crystallized phase proportion need to be estimated again. Indeed, the presence of nanodendrites in the glass induces that the composition of the glass would be better estimated with the use of a TEM apparatus equipped with a chemical analysis probe. With this technique it is possible to dismiss the region with an association and to favour the analysis of glass (s.s.). Studies evoke inhomogeneous iron contents in such glasses [69]. Then, by the use of TEM, it would be possible to verify if glass alteration is not homogeneously spread on the slag surface because of variations of the glass composition (e.g. iron contents).

A better characterization of the Fe-rich entities could be done by studying the magnetic properties of the waste. Indeed, magnetic susceptibility and high magnetic field measurements could give valuable indications to discuss about the presence of franklinite, wüstite or magnetite, their proportions and if they are Zn substituted (by analogy with plurimicrometric wüstite). Indeed, Zn contents in glass may have been overestimated in a same way compared to Fe, whereas it is an element which improves the glass chemical durability.

4.3. Alteration mechanisms

SEM-EDS investigations demonstrate that in such acidic near neutral environment, there are preferential releases of alkali and alkali-earth metals. This is relevant with numerous other studies dealing with glass leaching [14,51] because the main phase to react is the glass matrix. The altered glass layer is mainly composed of Si and Fe. Numerous papers indicate that iron, silicon and aluminium are preferentially incorporated in the altered layer or in secondary phases [15,24,26]. Preferential incorporation of iron has also been demonstrated in the glass matrix of archeological slags [70]. In oxidizing conditions, alteration mechanisms lead to the oxidation of ferrous into ferric iron. Such Fe(III) is relatively stable in the altered layer thanks too a very low solubility. However, Refs. [4] and [13] evoke the formation of iron oxy-hydroxide. In this work, excluding lead carbonates, no secondary phase has been observed. This is quite relevant with high flow rate and then lower saturation indexes [26]. Nevertheless, Pb retention mechanisms exist: pollutant adsorption onto altered glass (by Pb/alkali-earth metal exchanges) and adsorption onto crystallized phases.

5. Conclusions

As for a lot of vitrified or annealed iron-rich silica wastes, LBF slags contain widely submicron Fe-rich entities in its glass matrix. Previous studies and results presented here tend to confirm the presence of nanometric wüstite, franklinite or magnetite in significant amounts. Nevertheless, additional TEM-EDS investigations and the characterization of their magnetic properties are needed to better identify these phases and to propose a glass composition which take into account their presence. Alteration mechanisms of such waste is quite similar to others studies dealing with archaeological slags and glass leaching. In an open flow test with acidic near neutral environment, LBF glass matrix preferentially releases alkalis to form a Si and Fe enriched altered layer. The altered glass is heterogeneously distributed at the slag surface. This is linked to the dissolution of Pb-rich entities and could also be associated with glass composition variations (Zn, Fe, Ca, Si contents).

Acknowledgements

This work was supported by the French Environmental Agency (ADEME) and the Nord-Pas-de-Calais Regional Council (PRC Program, France). Thanks to Jacky Laureyns (LASIR) for his help concerning Raman peak identifications and to Miguel Vandaele and Patrick Degrugilliers for their valuable help and their advices, concerning the sample preparations.

References

[1] C. Mahé-Le-Carlier, Caractérisation pétrographique et chimique d'analogues de déchets vitrifiés actuels: les scories de la métallurgie ancienne, étude de l'altération naturelle et expérimentale, Ph.D. Thesis, Institut National Polytechnique de Lorraine, Nancy, France, 1997, 235 pp.

[2] C. Gee, M.H. Ramsey, J. Maskall, I. Thornton, Mineralogy and weathering processes in historical smelting slags and their effect on the mobilisation of lead, J. Geochem. Explor. 58 (1997) 249–257.

[3] V. Ettler, O. Legendre, F. Bodénan, J.C. Touray, Primary phases and natural wheathering of old lead-zinc pyrometallurgical slag from Pribram, Czech Republic, Can. Mineral. 39 (2001) 873–888.

[4] D. Deneele, Caractérisation, simulations expérimentales et thermodynamiques de l'altération de déchets vitreux: les scories de première fusion de plomb et de zinc, University Ph.D. Thesis, University of Lille 1, France, 2002, 187 pp.

[5] F. Verhaeghe, B. Blanpain, P. Wollants, 1D combined flow and thermodynamic modelling of a lead blast furnace, in: Proceedings of the Third International Conference on CFD in the Minerals and Process Industries, CSIRO, 2003, pp. 449–454.

[6] P. Verguts, A two-dimensional mathematical simulation model for a non-ferrous blast furnace, Ph.D. Thesis manuscript, Katholieke Universiteit Leuven, Belgium, 2005, 164 pp.

[7] C. Gervais, Evaluation environnementale des perspectives de valorisation en BTP de scories de première fusion de plomb et de zinc, Ph.D. Thesis, Institut National des Sciences Appliquées de Lyon, France, 1999, 218 pp.

[8] S. Sobanska, B. Ledésert, D. Deneele, A. Laboudigue, Alteration in soils of slag particules resulting from lead smelting, C. R. Acad. Sci. Paris, Earth Planet. Sci. 331 (2000) 271–278.

[9] R. Barna, P. Moszkowicz, C. Gervais, Leaching assessment of road materials containing primary lead and zinc slags, Waste Manage. 24 (2004) 945–955.

[10] V. Ettler, Z. Johan, J.C. Touray, E. Jelinek, Zinc partitioning between glass and silicate phases in historical and modern lead-zinc metallurgical slags from the Pribram district, Czech Republic, C. R. Acad. Sci. Earth Planet. Sci. 331 (2000) 245–250.

[11] A. Karamarov, M. Pelino, Crystallization phenomena in Fe-rich glasses, J. Non-Crystal. Solids 281 (2001) 139–151.

[12] V. Ettler, P. Piantione, J.C. Touray, Mineralogical control on inorganic contaminant mobility in leachate from lead-zinc metallurgical slag: experimental approach and long-term assessment, Mineral. Mag. 67 (2003) 1269–1283.

[13] V. Ettler, M. Komarkova, J. Jehlicka, P. Coufal, D. Hradil, V. Machovic, F. Delorme, Leaching of lead metallurgical slag in citric solutions—implications for disposal and weathering in soil environments, Chemosphere 57 (2004) 567–577.

[14] M.J. Eick, P.R. Grossl, D.C. Golden, D.L. Sparks, D.W. Ming, Dissolution kinetics of lunar glass simulant at 25 °C: the effect of pH and organic acids, Geochim. Cosmochim. Acta 60 (1996) 157–170.

[15] P.K. Abraitis, F.R. Livens, J.E. Monteith, J.S. Small, D.P. Trivedi, D.J. Vaughan, R.A. Wogelius, The kinetics and mechanisms of simulated British Magnox waste glass dissolution as a funtion of pH, silicic acid activity and time in low temperature aqueous systems, Appl. Geochem. 15 (2000) 1399–1416.

[16] T. Advocat, P. Jollivet, J.L. Crovisier, M. del Nero, Long-term alteration mechanisms in water for SON68 radioactive borosilicate glass, J. Nucl. Mater. 298 (2001) 55–62.

[17] S.R. Gislason, E.H. Oelkers, Mechanism, rates and consequences of basaltic glass dissolution. II: An experimental study of the dissolution rates of basaltic glass as a function of pH and temperature, Geochim. Cosmochim. Acta 67 (2003) 3817–3832.

[18] G.A. Hudson, F.R. Bacon, Inhibition of alkaline attack on soda-lime glass, J. Am. Ceram. Soc. 37 (1958) 185–188.

[19] C.Q. Buckwalter, L.R. Pederson, Inhibition of nuclear waste glass leaching by chemisorption, J. Am. Ceram. Soc. 65 (1982) 431–436.

[20] G.L. McVay, C.Q. Buckwalter, Effect of iron on waste-glass leaching, J. Am. Ceram. Soc. 66 (1983) 170–174.

[21] B. Grambow, A general rate equation for nuclear waste glass corrosion, Mater. Res. Soc. Symp. Proc. 44 (85) 15–27.

[22] P.K. Abraitis, B.P. McGrail, D.P. Trivedi, F.R. Livens, D.J. Vaughan, Single-pass flow-through experiments on a simulated waste glass in alkaline media at 40 °C. II: Experiments conducted with buffer solution contain-

ing controlled quantities of Si and Al, J. Nucl. Mater. 280 (2000) 206–215.
[23] E.H. Oelkers, S.R. Gislason, The mechanism, rates and consequences of basaltic glass dissolution. I: An experimental study of the dissolution rates of basaltic glass as a function of aqueous Al, Si and oxalic acid concentration at 20 °C and pH 3 and 11, Geochim. Cosmochim. Acta 65 (2001) 3671–3681.
[24] I. Techer, T. Advocat, J. Lancelot, J.M. Liotard, Dissolution kinetics of basaltic glasses: control by solution chemistry and protective effect of the alteration film, Chem. Geol. 176 (2001) 235–263.
[25] I. Munier, J.L. Crovisier, B. Grambow, B. Fritz, A. Clément, Modelling the alteration gel composition of simplified borosilicate glasses by precipitation of an ideal solid solution in equilibrium with the leachant, J. Nucl. Mater. 324 (2004) 97–115.
[26] V. Daux, C. Guy, T. Advocat, J.L. Crovisier, P. Stille, Kinetic aspects of basaltic glass dissolution at 90 °C: role of aqueous silicon and aluminium, Chem. Geol. 142 (1997) 109–126.
[27] P.K. Abraitis, B.P. McGrail, D.P. Trivedi, F.R. Livens, D.J. Vaughan, Single-pass flow-through experiments on a simulated waste glass in alkaline media at 40 °C. I: Experiments conducted at variable solution flow rate to glass surface area ratio, J. Nucl. Mater. 280 (2000) 196–205.
[28] A. Gauthier, P. Le Coustumer, M. Motelica-Heino, O.F.X. Donard, Real time alteration of a nuclear waste glass and remobilization of lanthanide into an interphase, Waste Manage. 20 (2000) 731–739.
[29] M. Tomozawa, C.Y. Erwin, M. Takata, E.B. Watson, Effect of water content on the chemical durability of Na_2O–$3SiO_2$ glass, J. Am. Ceram. Soc. 65 (1982) 182–183.
[30] P. Frugier, N. Godon, E. Vernaz, F. Larché, Influence of composition variations on the initial alteration rate of vitrified domestic waste incineration fly-ash, Waste Manage. 22 (2002) 137–142.
[31] D. Perret, J.L. Crovisier, P. Stille, G. Shields, U. Mäder, T. Advocat, K. Schenk, M. Chardonnens, Thermodynamic stability of waste glasses compared to leaching behaviour, Appl. Geochem. 18 (2003) 1165–1184.
[32] P. Frugier, C. Marin, I. Ribet, T. Advocat, S. Gin, The effect of composition on the leaching of three nuclear waste glasses: R7T7, AVM, VRZ, J. Nucl. Mater. 346 (2005) 194–207.
[33] W.H. Zachariasen, The atomic arrangement in glass, J. Am. Chem. Soc. 54 (1932) 3841–3851.
[34] G.N. Greaves, EXAFS, glass structure and diffusion, Philos. Mag. B 60 (1989) 793–800.
[35] C.H.L. Goodman, The structure and properties of glass and the strained mixed cluster model, Phys. Chem. Glasses 26 (1985) 1–10.
[36] M.D. Ingram, Relaxation processes in ionically conducting glasses, J. Non-Crystal. Solids 131–133 (1991) 995–1003.
[37] G. Calas, L. Cormier, L. Galoysis, P. Jollivet, Structure-property relationships in multi-component oxide glasses, C. R. Chim. 5 (2003) 1–13.
[38] P.H. Gaskell, Medium range order and random networks, J. Non-Crystal. Solids 293–295 (2001) 146–152.
[39] G.H. Frischat, J.F. Poggemann, G. Heide, Nanostructure and atomic structure of glass seen by atomic force microscopy, J. Non-Crystal. Solids 345/346 (2004) 197–202.
[40] G.N. Greaves, A. Fontaine, P. Lagarde, D. Raoux, S.J. Gurman, Local structure of silicate glasses, Nature 293 (1981) 611–616.
[41] F. Seifert, B.O. Mysen, D. Virgo, Three-dimensional network structure of quenched melts (glass) in the systems SiO_2–$NaAlO_2$, SiO_2–$CaAl_2O_4$ and SiO_2–$MgAl_2O_4$, Am. Mineral. 67 (1982) 696–717.
[42] M.C. Eckersley, P.H. Gaskell, A.C. Barnes, P. Chieux, Structural ordering in a calcium silicate glass, Nature 335 (1988) 525–527.
[43] L. Cormier, D. Ghaleb, D.R. Neuville, J.M. Delaye, G. Calas, Chemical dependence of network topology of calcium aluminosilicate glasses: a computer simulation study, J. Non-Crystal. Solids 332 (2003) 255–270.
[44] H. Scholze, Glass: Nature, Structure and Properties, Springer Verlag, 1990, 454 pp.
[45] D. Holland, A. Mekki, I.A. Gee, C.F. McConville, J.A. Johnson, C.E. Johnson, P. Appleyard, M. Thomas, The structure of sodium iron silicate glass—a multi-technique approach, J. Non-Crystal. Solids 253 (1999) 192–202.
[46] S. Rossano, A.Y. Ramos, J.M. Delaye, Environment of ferrous iron in CaFeSi2O6 glass: contributions of EXAFS and molecular dynamics, J. Non-Crystal. Solids 273 (2000) 48–52.
[47] F. Farges, Y. Lefrère, S. Rossano, A. Berthereau, G. Calas, G.E. Brown, The effet of redox state on the local structural environment of iron in silicate glasses: a combined XAFS spectroscopy, molecular dynamics, and bond valence study, J. Non-Crystal. Solids 244 (2004) 176–188.
[48] P.W. Wang, L. Zhang, Structural role of lead silicate glasses derived from XPS spectra, J. Non-Crystal. Solids 194 (1996) 129–134.
[49] J. Rybicki, A. Rybicka, A. Witkowska, G. Bergmanski, A. Di Cicco, M. Minicucci, G. Manchini, The structure of lead-silicate glasses: molecular dynamics and EXAFS studies, J. Phys.: Cond. Matter 13 (2001) 9781–9797.
[50] G. Della Mea, A. Gasparotto, M. Bettinelli, A. Montenero, A. Gasparotto, Chemical durability of zinc-containing glasses, J. Non-Crystal. Solids 84 (1986) 443–451.
[51] E. Vernaz, S. Gin, C. Jégou, I. Ribet, Present understanding of R7T7 glass alteration kinetics and their impact on long-term behavior modelling, J. Nucl. Mater. 298 (2001) 27–36.
[52] C. Jégou, S. Gin, F. Larché, Alteration kinetics of a simplified nuclear glass in an aqueous medium: effects of solution chemistry and of protective gel properties on diminishing the alteration rate, J. Nucl. Mater. 280 (2000) 216–229.
[53] K. Lemmens, The effect of clay on the dissolution of nuclear waste glass, J. Nucl. Mater. 298 (2001) 11–18.
[54] S. Gin, I. Ribet, M. Couillard, Role and properties of the gel formed during nuclear glass alteration: importance of gel formation conditions, J. Nucl. Mater. 298 (2001) 1–10.
[55] D. Rebiscoul, P. Frugier, S. Gin, A. Ayral, Protective properties and dissolution ability of the gel formed during nuclear glass alteration, J. Nucl. Mater. 342 (2005) 26–34.
[56] A. Gauthier, P. Le Coustumer, J.H. Thomassin, Nature and effect of the alteration layer during nuclear waste glass dissolution, Sci. Basis Nucl. Waste Manage. 713 (2002) 555–561.
[57] N. Seignez, D. Bulteel, D. Damidot, A. Gauthier, J.L. Potdevin, Weathering of metallurgical slag heaps: multi-experimental approach of the chemical behaviours of lead and zinc, Trans. Ecol. Environ. 92 (2006) 31–41.
[58] D.L.A. De Faria, S. Venâcio Silva, M.T. de Oliveira, Raman microspectroscopy of some iron oxides and oxyhydroxides, J. Raman Spectrosc. 28 (1997) 873–878.
[59] R.L. Frost, W. Martens, J.T. Kloprogge, Z. Ding, Raman spectroscopy of selected lead minerals of environmental significance, Spectrochim. Acta Part A 59 (2003) 2705–2711.
[60] S.V. Dimitrova, D.R. Mehandgiev, Lead removal from aqueous solutions by granulated blast-furnace slag, Water Res. 32 (1998) 3289–3292.
[61] S.V. Dimitrova, Use of granular slag columns for lead removal, Water Res. 36 (2002) 4001–4008.
[62] S.V. Dimitrova, Effect of the heat treatment on the morphology and sorption ability to metal ions of metallurgical slag, J. Mater. Sci. 36 (2001) 2639–2643.
[63] M.M. Benjamin, J.O. Leckie, Multiple-site adsorption of Cd, Cu, Zn, and Pb on amorphous iron oxyhydroxide, J. Colloid Interface Sci. 79 (1981) 209–221.
[64] K.J. Farley, D.A. Dzombak, F.M. Morel, A surface precipitation model for sorption of cations on metal oxides, J. Colloid Interface Sci. 106 (1985) 226–242.
[65] S.V. Dimitrova, Metal sorption on blast-furnace slag, Water Res. 30 (1996) 228–232.
[66] P. Pisciella, S. Crisucci, A. Karamanov, M. Pelino, Chemical durability of glasses obtained by vitrification of industrial wastes, Waste Manage. 21 (2001) 1–9.
[67] L. Galoisy, G. Calas, M.A. Arrio, High-resolution XANES spectra of iron in minerals and glasses: structural information from the pre-edge region, Chem. Geol. 174 (2001) 307–319.

[68] S.B. Donald, A.M. Swink, H.D. Schreiber, High iron ferric glass, J. Non-Crystal. Solids 352 (2006) 539–543.
[69] F. Pinakidou, M. Katsikini, E.C. Paloura, P. Kavouras, O. Kalogirou, Ph. Komninou, Th. Karakostas, Modification of the Fe-environment in Fe_2O_3 glass/glass ceramic systems containing Pb, Na and Si, Nucl. Instrum. Methods. Phys. Res. Section B: Beam Interact. Mater. Atoms 246 (2006) 170–175.
[70] C. Mahé-le Carlier, C. le Carlier de Veslud, A. Ploquin, J.J. Royer, L'altération naturelle des scories de la métallurgie ancienne: un analogue des déchets vitrifiés, C. R. Acad. Sci. Paris II 330 (2000) 179–184.